

Steering magnonic dynamics and permeability at exceptional points in a parity-time symmetric waveguide

Xi-guang Wang,^{†,‡} Guang-hua Guo,[†] and Jamal Berakdar^{*,‡}

[†] *School of Physics and Electronics, Central South University, Changsha 410083, China*

[‡] *Institut für Physik, Martin-Luther Universität Halle-Wittenberg, D-06120 Halle/Saale,
Germany*

E-mail: jamal.berakdar@physik.uni-halle.de

Abstract

Tuning the low-energy magnetic dynamics is a key element in designing novel magnetic metamaterials, spintronic devices and magnonic logic circuits. This study uncovers a new, highly effective way of controlling the magnetic permeability via shaping the magnonic properties in coupled magnetic waveguides separated by current carrying spacer with strong spin-orbit coupling. The spin-orbit torques exerted on the waveguides leads to an externally tunable enhancement of magnetic damping in one waveguide and a decreased damping in the other, constituting so a magnetic parity-time (PT) symmetric system with emergent magnetic properties at the verge of the exceptional point where magnetic gains/losses are balanced. In addition to controlling the magnetic permeability, phenomena inherent to PT-symmetric systems are identified, including the control on magnon power oscillations, nonreciprocal magnon propagation, magnon trapping and enhancement as well as the increased sensitivity to magnetic perturbation and abrupt spin reversal. These predictions are demonstrated analytically and confirmed

by full numerical simulations under experimentally feasible conditions. The position of the exceptional points and the strength of the spontaneous PT symmetry breaking can be tuned by external electric and/or magnetic fields. The roles of the intrinsic magnetic damping, and the possibility of an electric control via Dzyaloshinskii-Moriya interaction are exposed and utilized for mode dispersion shaping and magnon amplification and trapping. The results point to a new route to designing optomagnonic waveguides, traps, sensors, and circuits.

Keywords

Magnonic circuits, PT-symmetry breaking, spin orbit torque, non-Hermitian dynamics, Optomagnonics, magnetic switching

Introduction

Nanomagnetism is the backbone of spin-based memories, data processing and sensorics. In a generic magnet, the permeability, meaning the magnetic response to a weak external perturbation is governed by the behavior of the spin waves which are collective transverse oscillations (with their quantum termed magnon) around the ground state. Miniaturized magnonic logic circuits¹⁻⁶ and waveguides operated at low energy cost with negligible Ohmic losses were demonstrated. Furthermore, geometric confinements, nanostructuring, and material design allow a precise spectral shaping and guiding of magnons, which is reflected respectively in a modified magnetic response. Here we point out an approach based on a magnonic gain-loss mechanism in two waveguides with a normal-metal spacer. The two magnetic waveguides are coupled via the Ruderman-Kittel-Kasuya-Yosida (RKKY) interaction. Driving charge current in a spacer layer with a strong spin-orbit coupling (cf. 1(a)), spin orbit torques (SOTs) are exerted on the magnetizations of the waveguides. In effect, SOT adds to the intrinsic magnetic damping, as evident from Eq. (1). It is thus possible to achieve a case

where SOT-induced magnetic losses in one waveguide are balanced by antidamping in the other waveguide. This is a typical case of a PT-symmetric system as realized for instance in optical systems.⁷⁻¹² A hallmark of PT-symmetric systems is that, even if the underlying Hamiltonian is non-Hermitian, the eigenvalues may be real,¹³⁻¹⁵ and turn complex when crossing the "exceptional point" and entering the PT-symmetry broken phase upon varying a parametric dependence in the Hamiltonian. Examples were demonstrated in optics and photonics,^{8-12,16-21} optomechanics,^{22,23} acoustics^{24,25} and electronics.²⁶⁻²⁹ Also, PT-symmetric cavity magnon-polaritons were discussed involving phonon dissipation or electromagnetic radiation as well as parametric driving or SOT effects.³⁰⁻³⁵

Our main goal is the design and demonstration of PT-symmetric magnonic waveguides which are controllable by feasible external means that serve as a knob to tune the system across the exceptional point. In addition to the documented advantages of magnons, this would bring about new functionalities that can be integrated in optomagnonic, spintronic, and magnonic circuits.

Spin-torque driven PT-symmetric waveguides

Our magnon signal propagates along two magnetic waveguides (which define the \vec{x} direction) coupled via RKKY exchange interaction (cf. Fig. 1(a)). A charge current flowing in a spacer with a large spin Hall angle (such as Pt) applies a SOT $\vec{T}_1 \parallel \vec{y}$ on first waveguide enhancing the effective damping, and a SOT $\vec{T}_2 \parallel -\vec{y}$ on second waveguide weakening the effective damping. The polarization directions of the spin Hall effect induced transverse spin currents $\vec{T}_1 = \vec{z} \times \vec{j}_{\text{Pt}}$ in WG1 and $\vec{T}_2 = (-\vec{z}) \times \vec{j}_{\text{Pt}}$ in WG2, are related to the charge current density \vec{j}_{Pt} . In a generic ferromagnet and for the long wavelength spin excitations of interest here, to describe the magnetic dynamics it is sufficient to adopt a classical continuous approach and solve for the equations of motion of the magnetization vector fields $\vec{M}_p(\vec{r}, t)$ ($p = 1, 2$

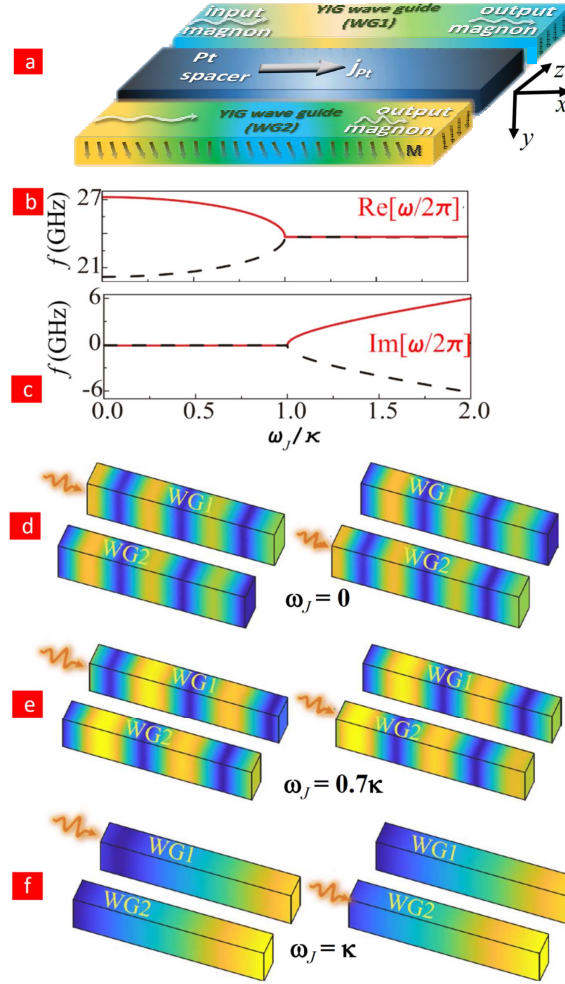


Figure 1: (a) Two magnetic waveguides (labeled as WG1 and WG2, as an example we use YIG in the numerical simulations) are coupled via RKKY interaction with metallic spacer that has a large spin Hall angle (here Pt). Driving a charge current \vec{j}_{Pt} along the space (x direction) results in spin-Hall torques acting on the magnetic waveguides. The torques damp or antidamp the magnetic dynamics in WG1 and WG2 resulting so in PT-symmetric structure with a new (PT) symmetry behavior of the magnetic permeability. Magnon wave packets are launched locally at one end of WG1 or WG2 (left side in the figure) and the propagation characteristics of the magnonic signal is steered, amplified or suppressed by external fields that drive the waveguides from the PT-symmetric to the PT-symmetry broken phase through the exceptional point where magnetic losses in WG1 balance magnetic antidamping in WG2. This can be achieved for instance by changing the ratio between the intrinsic coupling strength between the waveguides κ and the strength of the spin-Hall torques ω_J . (b) Real and (c) imaginary parts of two eigenmode frequency $f = \omega/(2\pi)$ as we scan ω_J/κ at the wave vector $k_x = 0.1 \text{ nm}^{-1}$. (d-f) Spatial profiles of propagating spin wave amplitude for different loss/gain balance (different ω_J), when the spin waves are locally excited either in WG1 or WG2. The color change from blue to red corresponds to a linear amplitude change ranging from 0 to the maximum of input signal. The local microwave field excites spin waves at the left side of the waveguide and has a frequency of 20 GHz. The length (along x axis) of waveguides in (d-f) is 580 nm.

enumerates the two waveguides), which amounts to propagating the Landau-Lifshitz-Gilbert (LLG) equation,^{36–39}

$$\frac{\partial \vec{M}_p}{\partial t} = -\gamma \vec{M}_p \times \vec{H}_{\text{eff},p} + \frac{\vec{M}_p}{M_s} \times \left[\alpha \frac{\partial \vec{M}_p}{\partial t} - \gamma c_J \vec{T}_p \times \vec{M}_p \right]. \quad (1)$$

The waveguides are located at $z = +z_0$ and $z = -z_0$. We are interested in small transversal excitations and hence it is useful to use the unit vector field $\vec{m}_p = \vec{M}_p/M_s$ where M_s is the saturation magnetization and γ is the gyromagnetic ratio. α is the conventional Gilbert damping inherent to magnetic losses in each of the waveguides. The effective field $\vec{H}_{\text{eff},p} = \frac{2A_{\text{ex}}}{\mu_0 M_s} \nabla^2 \vec{m}_p + \frac{J_{\text{RKKY}}}{2\mu_0 M_s t_p} \vec{m}_{p'} + H_0 \vec{y}$ consists of the internal exchange field, the interlayer RKKY coupling field, and the external magnetic field applied along the y axis, where $p, p' = 1, 2$, and $p' \neq p$. A_{ex} is the exchange constant, J_{RKKY} is the interlayer RKKY exchange coupling strength, t_p is the thickness of the p th layer, and μ_0 is the vacuum permeability. Of key importance to this study is the strength $c_J = T \theta_{\text{SH}} \frac{\hbar J_e}{2\mu_0 e t_p M_s}$ of SOT which is proportional to charge-current density J_e and the spin Hall angle θ_{SH} in the spacer layer, for instance, at the exceptional point defined in the following study, $c_J = 1 \times 10^5$ A/m corresponds to a charge current density of $J_e = 9 \times 10^8$ A/cm² in Pt.⁴⁰ T is the transparency at the interface, and e is the electron charge. Our proposal applies to a variety of settings, in particular synthetic antiferromagnets⁴¹ offer a good range of tunability. To be specific, we present here numerical simulations for Pt interfaced with a Yttrium-Iron-Garnet (YIG) waveguides as experimentally realized for instance in Ref. [40] corresponding to the following values $M_s = 1.4 \times 10^5$ A/m, $A_{\text{ex}} = 3 \times 10^{-12}$ J/m (technical details of the numerical realization are in the supplementary materials). For the Gilbert damping we use $\alpha = 0.004$ but note that depending on the quality of the waveguides α can be two order of magnitude smaller. The interlayer exchange constant $J_{\text{RKKY}} = 9 \times 10^{-5}$ J/m², which is in the typical range.⁴² For the waveguide thickness we used $t_{1,2} = 4$ nm. A large enough magnetic field $H_0 = 2 \times 10^5$ A/m is applied along $+y$ direction to bring the WGs to a remnant state.

Magnonic coupled wave-guide equations with spin-orbit torque

For a deeper understanding of the full-fledge numerical simulations presented below, it is instructive to formulate an analytical model by considering small deviations of $\vec{m}_{s,p} = (\delta m_{x,p}, 0, \delta m_{z,p})$ away from the initial equilibrium $\vec{m}_{0,p} = \vec{y}$. Introducing $\psi_p = \delta m_{x,p} + i\delta m_{z,p}$ we deduce from linearizing Eq. (1) the coupled waveguide equations

$$\begin{aligned} i\frac{\partial\psi_1}{\partial t} - [(\omega_0 - \alpha\omega_J) - i(\omega_J + \alpha\omega_0)]\psi_1 + q\psi_2 &= 0, \\ i\frac{\partial\psi_2}{\partial t} - [(\omega_0 + \alpha\omega_J) + i(\omega_J - \alpha\omega_0)]\psi_2 + q\psi_1 &= 0. \end{aligned} \quad (2)$$

For convenience, we introduce in addition to the coupling strength $q = \frac{\gamma J_{\text{RKKY}}}{(1+i\alpha)\mu_0 M_s t_p}$, the SOT coupling at zero intrinsic damping $\kappa = \gamma J_{\text{RKKY}}/(2\mu_0 M_s t_p) = q|_{\alpha \rightarrow 0}$. The intrinsic frequency of the waveguides is given by $\omega_0 = \frac{\gamma}{1+\alpha^2}(H_0 + \frac{2A_{\text{ex}}}{\mu_0 M_s}k_x^2 + \frac{J_{\text{RKKY}}}{2\mu_0 M_s t_p})$ which is for the material studied here is in the GHz. Essential for the behavior akin to PT-symmetric systems is the SOT-driven gain-loss term $\omega_J = \frac{\gamma c J}{1+\alpha^2}$. The wavevector along x direction is k_x . Eq. (2) admits a clear interpretation: The magnonic guided modes in the first waveguide (WG1) are subject to the confining complex potential $V(z) = V_R(z) + iV_i(z)$ with $V_R(z_0) = \omega_0 - \alpha\omega_J$ and $V_i(z_0) = -\omega_J - \alpha\omega_0$. In WG2 the potential is $V_R(-z_0) = \omega_0 + \alpha\omega_J$ and $V_i(-z_0) = \omega_J - \alpha\omega_0$. The mode coupling is mediated by q which determines the periodic magnon power exchange between WG1 and WG2 in absence of SOT.

For a PT symmetric system the condition $V_R(z_0) = V_R(-z_0)$ and $V_i(z_0) = -V_i(-z_0)$ must apply, which is obviously fulfilled if the intrinsic damping is very small ($\alpha \rightarrow 0$). Comparing the current and the photonic case, in the latter case the sign of the imaginary part of the WGs refractive index is tuned. Here we control with SOT the imaginary part of the permeability which we explicitly prove by deriving and analyzing of the magnetic susceptibility (cf. Supp. Materials). This finding points to a new route for designing PT-symmetric magneto-photonic structures via permeability engineering. We note, for a finite magnetic damping α a PT-

behavior is still viable as confirmed by the full numerical simulations that we discuss below.

Magnon dynamics across the spontaneous PT-symmetry breaking transition

The dispersion $\omega(k_x)$ of the modes governed by Eq. (2) reads

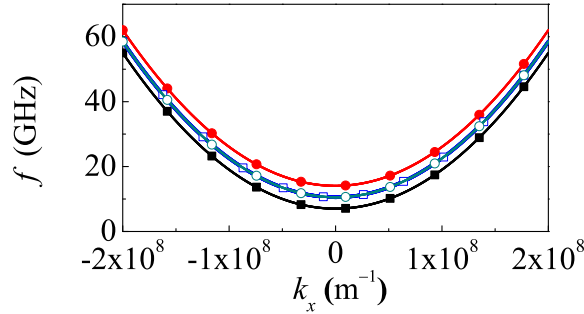


Figure 2: Merging of the acoustic ($\omega_J = 0$, solid squares) and optical magnon ($\omega_J = 0$, solid dots) modes dispersion $\text{Re}[\omega](k_x)$ when approaching the loss/gain-balanced exceptional point $\omega_J = \kappa$ (open dots).

$$\omega = (1 - i\alpha)\omega_0 \pm \sqrt{q^2 - \omega_J^2 + 2i\alpha\omega_J^2 + \alpha^2\omega_J^2} \quad (3)$$

which describes both the acoustic and optical magnon modes⁴³ and depends parametrically on ω_J and q . For $\alpha \rightarrow 0$ (in which case $q \equiv \kappa$) the eigenvalues are always real in the PT-symmetric regime below the gain/loss-balanced threshold $\omega_J/\kappa < 1$. At the exceptional point $\omega_J/\kappa = 1$, the two eigenvalues and eigenmodes become identical. For $\omega_J/\kappa > 1$ (by increasing the current density for instance) we enter the PT-symmetry broken phase, and the eigenvalues turn complex, as typical for PT-symmetric systems.^{21,44} The splitting between the two imaginary parts is determined by $2\kappa[(\omega_J/\kappa)^2 - 1]^{1/2}$ and is tunable by external fields. This fact is useful when exploiting the enhanced waveguides sensitivity to magnetic perturbations round the exceptional point. Allowing for a small damping α does not alter the modes behavior, as demonstrated by the full numerical results in a Fig. 1(b-c). The

full magnon dispersions ($\text{Re}[\omega]$ versus k_x curves) for $\omega_J/\kappa < 1$ and $\omega_J/\kappa = 1$ are shown in Fig. 2. The symmetry of our waveguide brings in a special behavior of the magnon signal transmission, meaning the propagation of a superposition of eigenmodes: Without charge current in the spacer ($\omega_J = 0$), a signal injected at one end in one waveguide oscillates between WG1 and WG2 (due to the coupling κ) in a manner that is well-established in coupled wave guide theory (cf. Fig. 1(d)). Switching on the charge current, ω_J/κ becomes finite and the beating of the magnon power between WG1 and WG2 increases (cf. Fig. 1(e)), as deducible from Eqs. (2), and also encountered in optical wave guides.⁴⁴ Eqs. (2) also indicate that near the exceptional point, a magnonic wavepacket injected in one waveguide no longer oscillates between the two waveguides but travels simultaneously in both waveguides, as confirmed in Fig. 1(f) by full numerical simulations. This behavior resembles the optics case.¹⁰ We note that in our waveguides, this limit is simply achieved by tuning the external electric and magnetic fields that then change the ratio ω_J/κ . We also found in line with Ref. [10] a non-reciprocal propagation below the exceptional point. Passing the exceptional point ($\omega_J/\kappa > 1$) the magnonic signal always propagates in the guide with gain and is quickly damped in the guide with loss.

Enhanced sensing at PT-symmetry breaking transition

To assess the susceptibility of our setup to external magnetic perturbations we apply an external microwave field \vec{h}_p which adds to effective field in the LLG equation. In frequency space we deduced that $\tilde{\psi}_p = \sum_{p'} \chi_{pp'} \gamma \tilde{h}_{m,p'}$ (tilde stands for Fourier transform), with $h_{m,p} = h_{x,p} + ih_{z,p}$, and $\chi_{pp'}$ is the dynamic magnetic susceptibility which has the matrix form

$$\chi = \frac{1}{(\omega_k - i\alpha\omega - \omega)^2 + \omega_c^2 - \kappa^2} \begin{pmatrix} (\omega_k - i\alpha\omega) + (i\omega_c - \omega) & \kappa \\ \kappa & (\omega_k - i\alpha\omega) - (i\omega_c - \omega) \end{pmatrix}, \quad (4)$$

with $\omega_c = \gamma c_J$ and $\omega_k = \gamma(H_0 + \frac{2A_{\text{ex}}k_x^2}{\mu_0 M_s} + \frac{J_{\text{RKKY}}}{2\mu_0 M_s t_p})$.

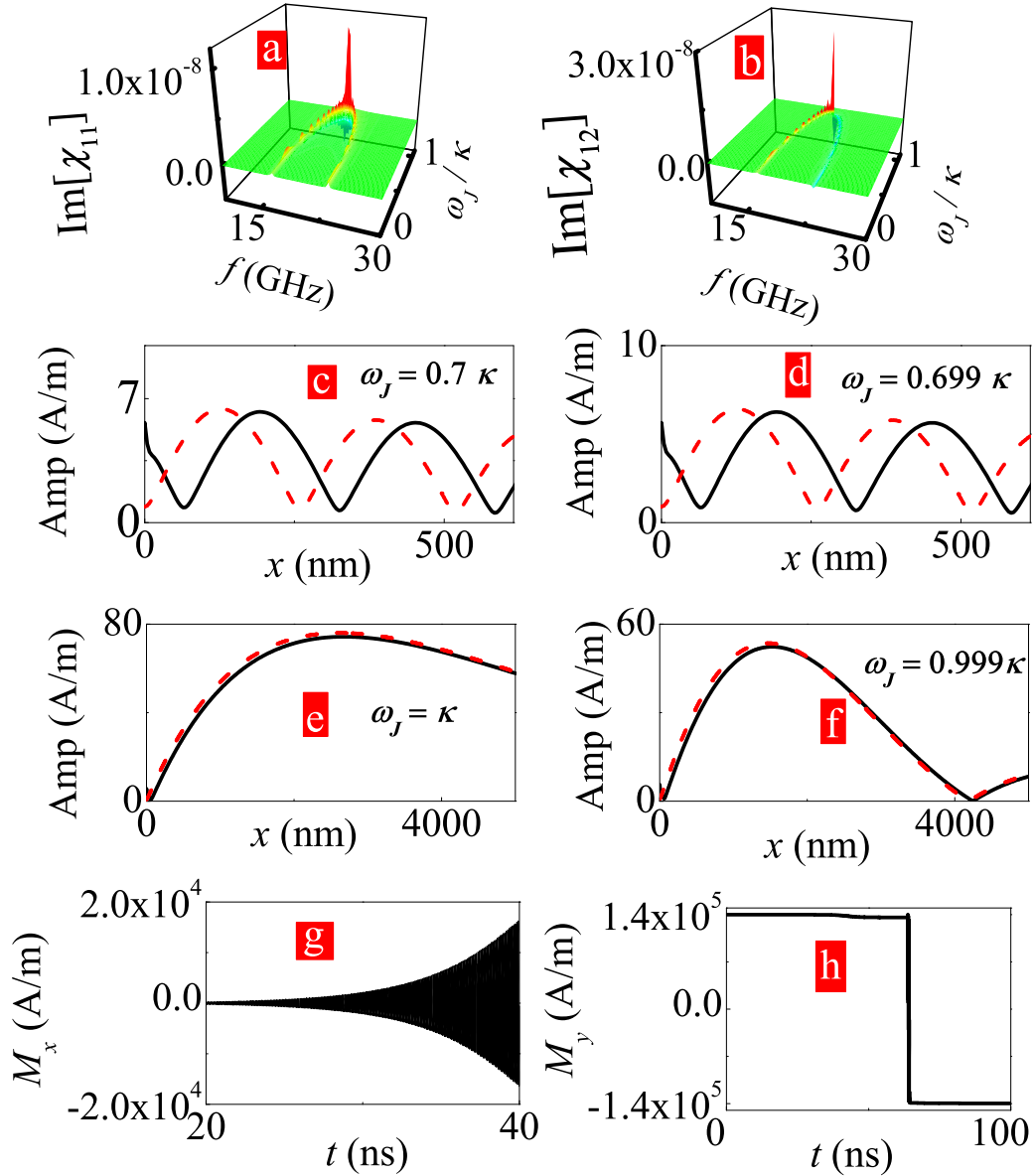


Figure 3: Magnetic susceptibility $\text{Im}[\chi_{11}]$ (a) and $\text{Im}[\chi_{12}]$ (b) as functions of f and ω_J . Peaks in $\text{Im}[\chi_{11}]$ and $\text{Im}[\chi_{12}]$ are found at the exceptional point $\omega_J = \kappa$. (c-f) Exciting spin waves of frequency 20 GHz at $x = 0$ in WG1, spatial profiles of spin wave amplitude for different ω_J . Black solid line and red dashed line represents the amplitudes in WG1 and WG2, respectively. Near $\omega = \kappa$, a slight variation in ω_J causes marked changes in the spin wave amplitudes (e-f), while the change is negligible near $\omega = 0.7\kappa$ (c-d). (g-h) At $\omega = \kappa$, increasing the external magnetic field ($H_0 = 2 \times 10^5$ A/m) in WG1 by 100 A/m, the time dependence of M_x (g) and M_y (h) at $x = 2000$ nm in WG2.

Near the exceptional point the system becomes strongly sensitive, for instance to changes in the charge current term ω_c , as testified by the behavior of the susceptibility which is demonstrated for the imaginary parts of χ_{11} and χ_{12} in Fig. 3. The high sensitivity of the excited spin waves on ω_c near the exception point (see Fig. 3(c-f)) is exploitable to detect slight changes in charge current density c_J .

Furthermore, near the exceptional point, our setup is strongly sensitive to changes in the magnetic environment. As an example, at $\omega_J = \kappa$, if the magnetic field H_0 (or local magnetization) is increased by 100 A/m in WG1, large amplitude spin-wave oscillations are generated in WG2, as evidenced by the time dependence of $M_x(x = 2000\text{nm})$ in WG2 (Fig. 3(g)). The spin wave amplification leads eventually to a reversal of M_y in WG2 (Fig. 3(h)). Away from the PT-breaking transition, e.g. for $\omega_J = 0.7\kappa$, when H_0 is reduced by the same amount in WG1, virtually no changes in propagating spin waves are observed (not shown). Obviously, this magnon amplification may serve as a tunable sensor for the magnetic environment.

Current-induced switching in magnetic PT-symmetric junctions

A special feature of magnetic systems is the possibility of current-induced switching (described by Eq. (1) but not by Eqs. (2)).⁴⁵ In fact, for large current densities we are well above the exceptional point. In this case the magnetic system becomes unstable towards switching. We find with further increasing the charge current density (enhancing ω_J), the local magnetization in guide 2 is indeed switched to $-y$. Magnon dynamics above the exceptional point is still possible however by tuning the spacer material properties or its thickness to obtain a smaller κ , for instance with $J_{\text{RKKY}} = 9 \times 10^{-7} \text{ J/m}^2$ and $\alpha = 0.01$. In this case the condition $\omega_J \gg \alpha\omega_0$ is not satisfied anymore, and the influence of intrinsic magnetic losses (α) in both wave guides is important. Nonetheless, even without reaching the strict

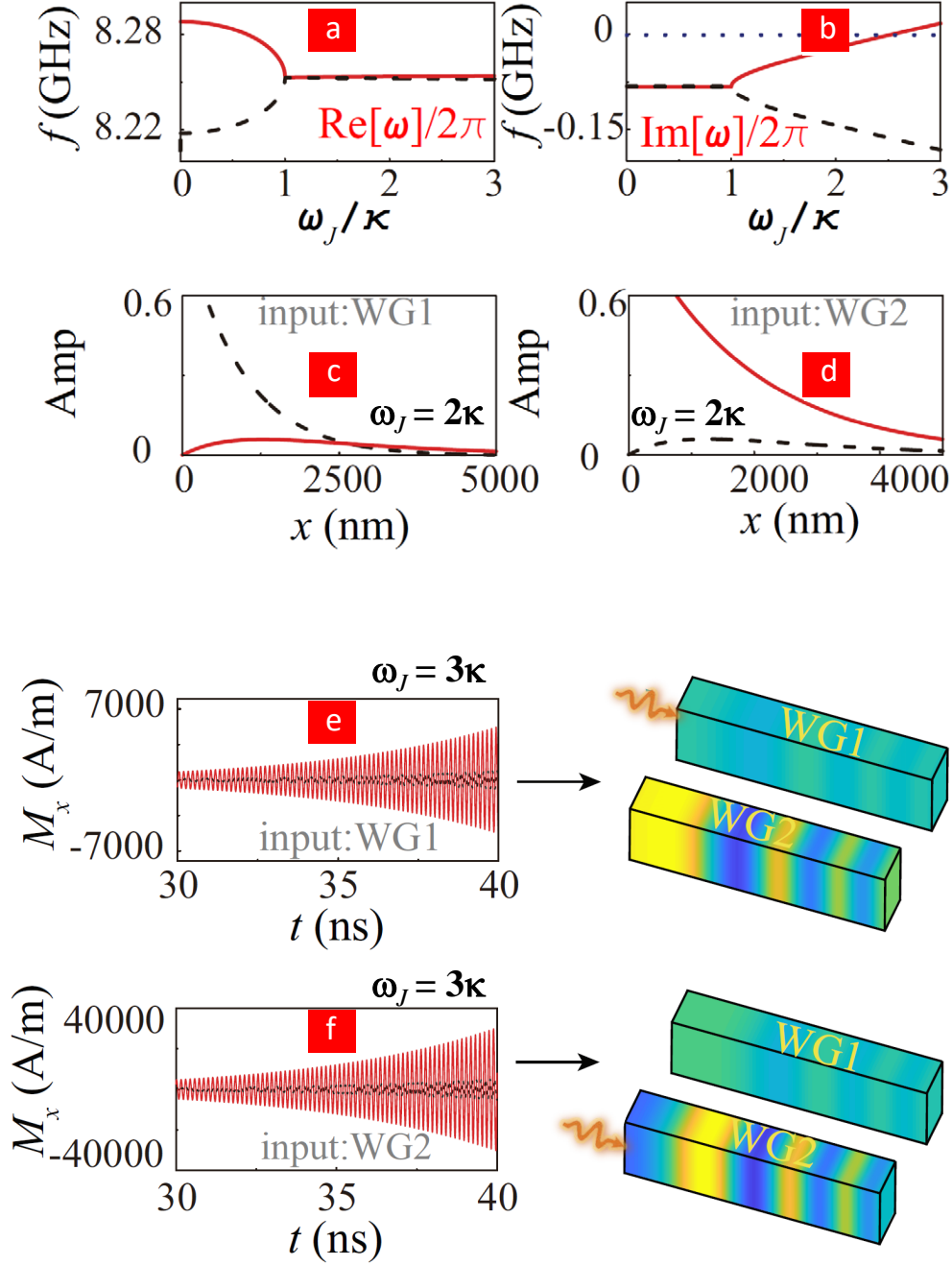


Figure 4: (a-b) Real and imaginary parts of the eigenmodes ω as varying the loss/gain balance by scanning ω_J (meaning, the SOT strength). The wave vector is $k_x = 0.03 \text{ nm}^{-1}$ and the intrinsic coupling between WG1 and WG2 κ is lowered, as compared to Fig. 1 (by choosing $J_{\text{RKKY}} = 9 \times 10^{-7} \text{ J/m}^2$). (c-d) Spatial profiles of magnon wave amplitudes (as normalized to their maxima) for $\omega_J = 2\kappa$, and ($\text{Re}[\omega] = 2\pi \times 20 \text{ GHz}$). Black dashed lines corresponds to WG1 and red solid line to WG2. (e-f) Time dependence (at the location $x = 2000 \text{ nm}$) and the spatial profiles (at $t = 40 \text{ ns}$) of the x component of the magnetization M_x for $\omega_J = 3\kappa$. The color variation from blue to red corresponds to a M_x change from the negative maximum to the positive maximum.

PT-symmetric condition, we still observe that the real parts of the two eigenvalues merge at the same point $\omega_J = \kappa$, and the two imaginary parts become different when $\omega_J > \kappa$, as shown by Fig. 4(a-b). When $\omega_J = 2\kappa$, the two imaginary parts are both negative, meaning that both modes are evanescent. The propagation of magnonic signal launched in one waveguide end is shown in Fig. 4 (c-d) evidencing that the spin waves in the two waveguides decay differently. An input signal in the waveguide with enhanced damping leads to an evanescent spin wave in WG1. Injecting the signal in WG2, the attenuation of spin wave is weaker, and its amplitude is always larger. When $\omega_J = 3\kappa$ and $\text{Im}[\omega]$ of the optical magnon mode turns positive, we observe that SOT induces spin wave amplification with time (Fig. 4(e-f)). This finding is interesting for cavity optomagnonics.⁴⁶

For input signal in WG1 or WG2, the spin wave amplitude is always larger in WG2 with a negative effective damping. Also, the excited spin wave amplitude is much larger when the input is in the WG2. Thus, no matter from which waveguide we start, the output signal is always distributed at the end of WG2, a fact that can be employed for constructing magnonic logic gates.

Dzyaloshinskii-Moriya interaction in electrically controlled PT-symmetric waveguides

In magnetic layers and at their interfaces an antisymmetric exchange, also called Dzyaloshinskii-Moriya (DM), interaction^{47,48} may exist. In our context it is particularly interesting that the DM interaction may allow for a coupling to an external electric field \vec{E} and voltage gates. The contribution to the system free energy density in the presence of DM and \vec{E} is $E_{elec} = -\vec{E} \cdot \vec{P}$, with the spin-driven polarization $\vec{P} = c_E[(\vec{m} \cdot \nabla)\vec{m} - \vec{m}(\nabla \cdot \vec{m})]$.^{49,50} This alters the magnon dynamics through the additional term $\vec{H}_{elec} = -\frac{1}{\mu_0 M_s} \frac{\delta E_{elec}}{\delta \vec{m}}$ in the effective field \vec{H}_{eff} . To uncover the role of DM interaction on the magnon dynamics in PT symmetric waveguides we consider three cases: (i) The two waveguides experience the same

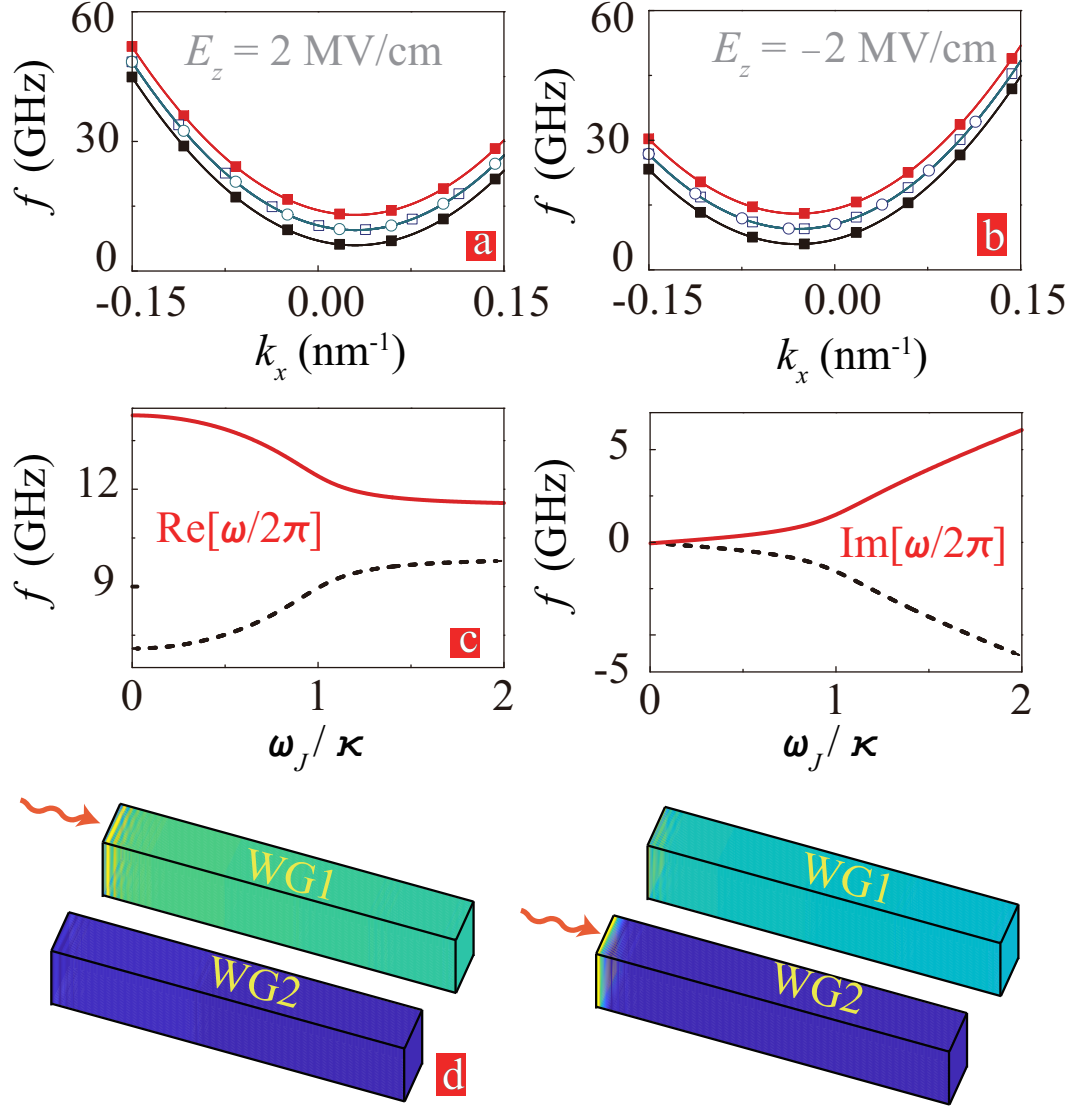


Figure 5: Control of coupled magnonic waveguide characteristics by an external electric field in presence of Dzyaloshinskii-Moriya interaction. (a-b) Applying a static electric field $\vec{E}_{1,2} = (0, 0, E_z)$ with $E_z = \pm 2$ MV/cm to both waveguides modify the magnon dispersion $\text{Re}[\omega](k_x)$ curves for $\omega_J = 0$ (solid dots) and $\omega_J = \kappa$ (open dots). (c) Real and imaginary parts of two eigenmodes ω as functions of ω_J and in the presence of two static electric fields (or voltages) applied with opposite polarity to the two waveguides ($\vec{E}_1 = (0, 0, E_z)$ and $\vec{E}_2 = (0, 0, -E_z)$, and $E_z = 2$ MV/cm) at $k_x = 0.1$ nm⁻¹. (d) Spatial profiles of the propagating spinwave amplitudes when applying electric field in WG1 ($\vec{E}_1 = (0, 0, E_z)$ with $E_z = 2$ MV/cm, and $\vec{E}_2 = (0, 0, 0)$). Color scale from blue to red corresponds to amplitude change from 0 to its maximum.

static electric field $\vec{E}_{1,2} = (0, 0, E_z)$.

(ii) The electric fields in the two waveguides are opposite to each other, i.e. $\vec{E}_1 = (0, 0, E_z)$ and $\vec{E}_2 = (0, 0, -E_z)$.

(iii) The electric field is applied only to waveguide 1. These situations can be achieved by electric gating.

For the case (i) with $\vec{E}_{1,2} = (0, 0, E_z)$, $\omega_0 = \frac{\gamma}{1+\alpha^2}(H_0 - \frac{2c_E E_z k_x}{\mu_0 M_s} + \frac{2A_{\text{ex}}}{\mu_0 M_s} k_x^2 + \frac{J_{\text{RKKY}}}{2\mu_0 M_s t_p})$ in Eq. 2, and the condition for PT-symmetry still holds. Applying an electric field along the z axis causes an asymmetry in the magnon dispersion. As shown by Fig. 5, the positive E_z shifts the dispersion towards positive k_x while a negative E_z shifts it in the opposite direction. With increasing ω_J , the changes of $\text{Re}[\omega]$ and $\text{Im}[\omega]$ (not shown) are similar to these in Fig. 1(b-c).

As for the case $\vec{E}_1 = (0, 0, E_z)$ and $\vec{E}_2 = (0, 0, -E_z)$, in the two equations (2) ω_0 is different. Explicitly: $\omega_0 = \frac{\gamma}{1+\alpha^2}(H_0 \mp \frac{2c_E E_z k_x}{\mu_0 M_s} + \frac{2A_{\text{ex}}}{\mu_0 M_s} k_x^2 + \frac{J_{\text{RKKY}}}{2\mu_0 M_s t_p})$ where the $-$ sign applies for WG1 and the $+$ sign corresponds to WG2. Hence, under an asymmetric electric field the potential V_R is not even ($V_R(z_0) \neq V_R(-z_0)$), and the PT-symmetry condition can not be satisfied. The ω_J dependence of $\text{Re}[\omega]$ and $\text{Im}[\omega]$ are shown in Fig 5, and no exceptional point can be strictly identified in this case.

For case (iii), we set $\vec{E}_1 = (0, 0, E_z)$ and $\vec{E}_2 = (0, 0, 0)$. The PT-symmetry condition is not satisfied. When the electric field is applied only to a single guide, it shifts selectively the magnon dispersion relation in this guide. Therefore, the magnon wave in the lower frequency range propagates solely in the guide with the electric field. As shown in Fig. 5(d), we excite the magnonic wavepacket with a frequency in the WG1 or WG2, the magnonic wave always propagates in the waveguide 1 which amounts to a magnon channeled by the electric field, while the propagation in the other guide is suppressed. This example illustrates yet another handle to steer magnonic waves swiftly and at low energy consumption by pulsed electric gating.

Conclusions

Magnonic waveguides based on magnetic junctions that exhibit a transition from a PT-symmetric to a PT-symmetry broken phase may act near the transition (exceptional) point as effective sensor for changes in external fields and in the magnetic environments and also serve as magnonic amplifier or magnetic switch. The particular behavior of the waveguides magnetic susceptibility is also reflected in the permeability (cf. supplementary materials) pointing to a new route to PT-symmetric magneto-photonics. Magnonic propagation is highly controllable by external electric and magnetic fields that can derive the system across the exceptional point and lead to controlled power distribution in the waveguides as well as non-reciprocal or amplified magnon waves. DM interaction allows for dispersion engineering via external electric fields, and for PT-symmetry based large-amplitude spin excitations. These observations underline the potential of PT-symmetric magnonics as the basis for additional functionalities of magnetophotonic, spintronics and cavity magnonic devices that are highly controllable by external parameters.

Acknowledgement

This research is financially supported by the DFG through SFB 762 and SFB TRR227, National Natural Science Foundation of China (No. 11704415, 11674400, 11374373), and the Natural Science Foundation of Hunan Province of China (No. 2018JJ3629).

Author contributions

XGW performed all numerical simulations and analytical modeling. JB conceived and supervised the project. XGW and JB wrote the paper. XGW, JB, and GHG discussed, interpret and agreed on the content.

Competing interests:

The authors declare no competing

financial and non-financial interests.

Full data availability statements: All technical details for producing the figures are enclosed in the supplementary materials. Data are available from the authors upon request.

Supporting Information Available

The following files are available free of charge.

- pt-symmetry-supp.pdf: Numerical simulation details, dynamic magnetic permeability in separated waveguides, and the influence of intrinsic damping.

References

- (1) Chumak, A. V.; Vasyuchka, V. I.; Serga, A. A.; Hillebrands, B. Magnon spintronics. *Nat. Phys.* **2015**, *11*, 453–461.
- (2) Wang, Q.; Pirro, P.; Verba, R.; Slavin, A.; Hillebrands, B.; Chumak, A. V. Reconfigurable nanoscale spin-wave directional coupler. *Sci. Adv.* **2018**, *4*, e1701517.
- (3) Kruglyak, V. V.; Demokritov, S. O.; Grundler, D. Magnonics. *J. Phys. D: Appl. Phys.* **2010**, *43*, 264001.
- (4) Vogt, K.; Fradin, F. Y.; Pearson, J. E.; Sebastian, T.; Bader, S. D.; Hillebrands, B.; Hoffmann, A.; Schultheiss, H. Realization of a spin-wave multiplexer. *Nat. Commun.* **2014**, *5*, 3727.
- (5) Chumak, A. V.; Serga, A. A.; Hillebrands, B. Magnon transistor for all-magnon data processing. *Nat. Commun.* **2014**, *5*, 4700.
- (6) Sadovnikov, A. V.; Beginin, E. N.; Sheshukova, S. E.; Romanenko, D. V.; Sharaevskii, Y. P.; Nikitov, S. A. Directional multimode coupler for planar magnonics: Side-coupled magnetic stripes. *Appl. Phys. Lett.* **2015**, *107*, 202405.

- (7) Ruschhaupt, A.; Delgado, F.; Muga, J. G. Physical realization of \mathcal{PT} -symmetric potential scattering in a planar slab waveguide. *J. Phys. A* **2005**, *38*, L171–L176.
- (8) Feng, L.; Wong, Z. J.; Ma, R.-M.; Wang, Y.; Zhang, X. Single-mode laser by parity-time symmetry breaking. *Science* **2014**, *346*, 972–975.
- (9) Makris, K. G.; El-Ganainy, R.; Christodoulides, D. N.; Musslimani, Z. H. Beam Dynamics in \mathcal{PT} Symmetric Optical Lattices. *Phys. Rev. Lett.* **2008**, *100*, 103904.
- (10) Rüter, C. E.; Makris, K. G.; El-Ganainy, R.; Christodoulides, D. N.; Segev, M.; Kip, D. Observation of parity-time symmetry in optics. *Nat. Phys.* **2010**, *6*, 192–195.
- (11) Regensburger, A.; Bersch, C.; Miri, M.-A.; Onishchukov, G.; Christodoulides, D. N.; Peschel, U. Parity-time synthetic photonic lattices. *Nature* **2012**, *488*, 167–171.
- (12) Zhang, X.-L.; Wang, S.; Hou, B.; Chan, C. T. Dynamically Encircling Exceptional Points: In situ Control of Encircling Loops and the Role of the Starting Point. *Phys. Rev. X* **2018**, *8*, 021066.
- (13) Bender, C. M.; Boettcher, S. Real Spectra in Non-Hermitian Hamiltonians Having \mathcal{PT} Symmetry. *Phys. Rev. Lett.* **1998**, *80*, 5243–5246.
- (14) Bender, C. M.; Brody, D. C.; Jones, H. F. Complex Extension of Quantum Mechanics. *Phys. Rev. Lett.* **2002**, *89*, 270401.
- (15) Bender, C. M. Making sense of non-Hermitian Hamiltonians. *Rep. Prog. Phys.* **2007**, *70*, 947–1018.
- (16) Peng, B.; Özdemir, S. K.; Lei, F.; Monifi, F.; Gianfreda, M.; Long, G. L.; Fan, S.; Nori, F.; Bender, C. M.; Yang, L. Parity-time-symmetric whispering-gallery microcavities. *Nat. Phys.* **2014**, *10*, 394–398.

- (17) Lin, Z.; Ramezani, H.; Eichelkraut, T.; Kottos, T.; Cao, H.; Christodoulides, D. N. Unidirectional Invisibility Induced by \mathcal{PT} -Symmetric Periodic Structures. *Phys. Rev. Lett.* **2011**, *106*, 213901.
- (18) Nazari, F.; Nazari, M.; Moravvej-Farshi, M. K. A 2×2 spatial optical switch based on PT-symmetry. *Opt. Lett.* **2011**, *36*, 4368–4370.
- (19) Kartashov, Y. V.; Szameit, A.; Vysloukh, V. A.; Torner, L. Light tunneling inhibition and anisotropic diffraction engineering in two-dimensional waveguide arrays. *Opt. Lett.* **2009**, *34*, 2906–2908.
- (20) Miri, M.-A.; Regensburger, A.; Peschel, U.; Christodoulides, D. N. Optical mesh lattices with \mathcal{PT} symmetry. *Phys. Rev. A* **2012**, *86*, 023807.
- (21) Guo, A.; Salamo, G. J.; Duchesne, D.; Morandotti, R.; Volatier-Ravat, M.; Aimez, V.; Siviloglou, G. A.; Christodoulides, D. N. Observation of \mathcal{PT} -Symmetry Breaking in Complex Optical Potentials. *Phys. Rev. Lett.* **2009**, *103*, 093902.
- (22) Lü, X.-Y.; Jing, H.; Ma, J.-Y.; Wu, Y. \mathcal{PT} -Symmetry-Breaking Chaos in Optomechanics. *Phys. Rev. Lett.* **2015**, *114*, 253601.
- (23) Xu, H.; Mason, D.; Jiang, L.; Harris, J. G. E. Topological energy transfer in an optomechanical system with exceptional points. *Nature* **2016**, *537*, 80–83.
- (24) Zhu, X.; Ramezani, H.; Shi, C.; Zhu, J.; Zhang, X. \mathcal{PT} -Symmetric Acoustics. *Phys. Rev. X* **2014**, *4*, 031042.
- (25) Fleury, R.; Sounas, D.; Alù, A. An invisible acoustic sensor based on parity-time symmetry. *Nat. Commun.* **2015**, *6*, 5905.
- (26) Schindler, J.; Li, A.; Zheng, M. C.; Ellis, F. M.; Kottos, T. Experimental study of active LRC circuits with \mathcal{PT} symmetries. *Phys. Rev. A* **2011**, *84*, 040101.

- (27) Schindler, J.; Lin, Z.; Lee, J. M.; Ramezani, H.; Ellis, F. M.; Kottos, T. \mathcal{PT} -symmetric electronics. *J. Phys. A* **2012**, *45*, 444029.
- (28) Assawaworrarit, S.; Yu, X.; Fan, S. Robust wireless power transfer using a nonlinear parity-time-symmetric circuit. *Nature* **2017**, *546*, 387–390.
- (29) Chen, P.-Y.; Sakhdari, M.; Hajizadegan, M.; Cui, Q.; Cheng, M. M.-C.; El-Ganainy, R.; Alù, A. Generalized parity-time symmetry condition for enhanced sensor telemetry. *Nat. Electron.* **2018**, *1*, 297–304.
- (30) Lee, J. M.; Kottos, T.; Shapiro, B. Macroscopic magnetic structures with balanced gain and loss. *Phys. Rev. B* **2015**, *91*, 094416.
- (31) Galda, A.; Vinokur, V. M. Parity-time symmetry breaking in magnetic systems. *Phys. Rev. B* **2016**, *94*, 020408.
- (32) Galda, A.; Vinokur, V. M. Parity-time symmetry breaking in spin chains. *Phys. Rev. B* **2018**, *97*, 201411.
- (33) Zhang, D.; Luo, X.-Q.; Wang, Y.-P.; Li, T.-F.; You, J. Q. Observation of the exceptional point in cavity magnon-polaritons. *Nat. Commun.* **2017**, *8*, 1368.
- (34) Cao, Y.; Yan, P. Exceptional magnetic sensitivity of \mathcal{PT} -symmetric cavity magnon polaritons. *Phys. Rev. B* **2019**, *99*, 214415.
- (35) Yang, H.; Wang, C.; Yu, T.; Cao, Y.; Yan, P. Antiferromagnetism Emerging in a Ferromagnet with Gain. *Phys. Rev. Lett.* **2018**, *121*, 197201.
- (36) Krivorotov, I. N.; Emley, N. C.; Sankey, J. C.; Kiselev, S. I.; Ralph, D. C.; Buhrman, R. A. Time-Domain Measurements of Nanomagnet Dynamics Driven by Spin-Transfer Torques. *Science* **2005**, *307*, 228–231.

- (37) Liu, L.; Lee, O. J.; Gudmundsen, T. J.; Ralph, D. C.; Buhrman, R. A. Current-Induced Switching of Perpendicularly Magnetized Magnetic Layers Using Spin Torque from the Spin Hall Effect. *Phys. Rev. Lett.* **2012**, *109*, 096602.
- (38) Garello, K.; Miron, I. M.; Avci, C. O.; Freimuth, F.; Mokrousov, Y.; Blügel, S.; Auffret, S.; Boule, O.; Gaudin, G.; Gambardella, P. Symmetry and magnitude of spin-orbit torques in ferromagnetic heterostructures. *Nat. Nanotechnol.* **2013**, *8*, 587–593.
- (39) Hoffmann, A. Spin Hall Effects in Metals. *IEEE Trans. Magn.* **2013**, *49*, 5172–5193.
- (40) Collet, M.; de Milly, X.; d’Allivy Kelly, O.; Naletov, V. V.; Bernard, R.; Bortolotti, P.; Ben Youssef, J.; Demidov, V. E.; Demokritov, S. O.; Prieto, J. L.; Muñoz, M.; Cros, V.; Anane, A.; de Loubens, G.; Klein, O. Generation of coherent spin-wave modes in yttrium iron garnet microdiscs by spin-orbit torque. *Nat. Commun.* **2016**, *7*, 10377.
- (41) Duine, R. A.; Lee, K.-J.; Parkin, S. S. P.; Stiles, M. D. Synthetic antiferromagnetic spintronics. *Nat. Phys.* **2018**, *14*, 217–219.
- (42) Heinrich, B.; Burrowes, C.; Montoya, E.; Kardasz, B.; Girt, E.; Song, Y.-Y.; Sun, Y.; Wu, M. Spin Pumping at the Magnetic Insulator (YIG)/Normal Metal (Au) Interfaces. *Phys. Rev. Lett.* **2011**, *107*, 066604.
- (43) Konovalenko, A.; Lindgren, E.; Cherepov, S. S.; Korenivski, V.; Worledge, D. C. Spin dynamics of two-coupled nanomagnets in spin-flop tunnel junctions. *Phys. Rev. B* **2009**, *80*, 144425.
- (44) Klaiman, S.; Günther, U.; Moiseyev, N. Visualization of Branch Points in \mathcal{PT} -Symmetric Waveguides. *Phys. Rev. Lett.* **2008**, *101*, 080402.
- (45) Baumgartner, M.; Garello, K.; Mendil, J.; Avci, C. O.; Grimaldi, E.; Murer, C.; Feng, J.; Gabureac, M.; Stamm, C.; Acremann, Y.; Finizio, S.; Wintz, S.; Raabe, J.; Gam-

- bardella, P. Spatially and time-resolved magnetization dynamics driven by spin-orbit torques. *Nat. Nanotechnol.* **2017**, *12*, 980–986.
- (46) Osada, A.; Hisatomi, R.; Noguchi, A.; Tabuchi, Y.; Yamazaki, R.; Usami, K.; Sadgrove, M.; Yalla, R.; Nomura, M.; Nakamura, Y. Cavity Optomagnonics with Spin-Orbit Coupled Photons. *Phys. Rev. Lett.* **2016**, *116*, 223601.
- (47) Zakeri, K.; Zhang, Y.; Prokop, J.; Chuang, T.-H.; Sakr, N.; Tang, W. X.; Kirschner, J. Asymmetric Spin-Wave Dispersion on Fe(110): Direct Evidence of the Dzyaloshinskii-Moriya Interaction. *Phys. Rev. Lett.* **2010**, *104*, 137203.
- (48) Moon, J.-H.; Seo, S.-M.; Lee, K.-J.; Kim, K.-W.; Ryu, J.; Lee, H.-W.; McMichael, R. D.; Stiles, M. D. Spin-wave propagation in the presence of interfacial Dzyaloshinskii-Moriya interaction. *Phys. Rev. B* **2013**, *88*, 184404.
- (49) Wang, X.-g.; Chotorlishvili, L.; Guo, G.-h.; Berakdar, J. High-Fidelity Magnonic Gates for Surface Spin Waves. *Phys. Rev. Applied* **2019**, *12*, 034015.
- (50) Zhang, X.; Liu, T.; Flatté, M. E.; Tang, H. X. Electric-Field Coupling to Spin Waves in a Centrosymmetric Ferrite. *Phys. Rev. Lett.* **2014**, *113*, 037202.